shown as a function of fluid feed pressure and capillary voltage. The dashed lines enclose the region for which stable, well focused, axial beams were obtained. Within this region, pressure and voltage could be varied to give a continuous range of charge to mass ratios. At each of the operating points indicated in the figure, several TOF measurements were made at different times, with the source being brought to the desired pressure and voltage from a variety of different initial values. While there was a degree of nonreproducibility the average values of the charge to mass ratio over the various measurements were quite consistent and were useful as indicators of the probable value to be achieved at a given operating point. It appeared that the use of Pt—Ir capillaries led to more reproducible results than could be obtained with stainless steel capillaries. The average values are shown beside each of the operating points in Fig. 1. By interpolation between points, contours of constant charge to mass ratio have been estimated.

Stable and consistent source operation, similar to that indicated in Fig. 1 has been observed over the complete range of capillary sizes and fluid doping levels previously mentioned. For each different source a stable and axially focused beam was produced between about 13 kV and 20 kV for fluid feed pressures between 2 cm Hg and 18 cm Hg. The associated charge to mass ratios of the beams, which depends on the capillary size, on the operating pressure and voltage and on the amount of doping, varied between about 10 coul/kg and 100 coul/kg. High pressure and low voltage gave the lowest charge to mass ratios while low pressure and high voltage gave the highest values. Smaller capillary tubes and higher doping levels tended to yield consistently higher charge to mass ratios.

Figures 2a and 2b show the spatial distribution of a typical beam in the axially focused region. The beam was produced at a capillary voltage of 20 kV using a 0.18 mm i.d. by 0.41 mm o.d. Pt—Ir capillary tube, 5 g NaI/10 ml glycerol fluid, and a fluid feed pressure of 7.8 cm Hg. Figure 2a is a photograph of the beam incident on the phosphor detector. Figure 2b shows the corresponding current measured at each segment of the concentric ring detector. Both detectors were at the same distance from the source. About 65% of the beam current lies within a cone that makes a half angle of 5° with the detector axis. Negligible current was detected beyond 15°.

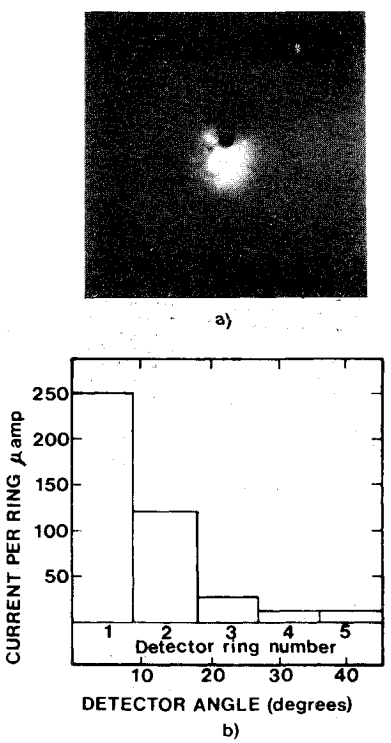

Fig. 2 a) Phosphor screen detector display of a beam produced at a capillary voltage of 20 kV using a 0.18 mm i.d. by 0.41 mm o.d. Pt—Ir capillary tube, a 5 g NaI/100 ml glycerol fluid and a feed pressure of 7.8 cm Hg. b) Current distribution of the above beam as measured on the concentric ring TOF detector.

These results indicate that a colloid source of conventional design can produce well focused axial beams with narrow distributions of charge to mass ratio by using relatively large capillary voltages and lowly doped working fluids. In this way it is possible to produce high quality colloid beams for use in reliable and efficient microthrust rockets. Such beams are also of interest in micrometeoroid simulation,[9,10] and in microparticle-surface interactions which may hold potential for producing plasma and fusion phenomena.[11]

References

[1] Kidd, P. W., "Parametric Studies with a Single-Needle Colloid Thruster," *Journal of Spacecraft and Rockets*, Vol. 5, No. 9, Sept. 1968, pp. 1034–1039.

[2] Huberman, M. N. and Cohen, E., "Research on Charged Particle Electrostatic Thrusters," AFAPL-TR-67-115, 1967, Aero Propulsion Labs., Wright-Patterson Air Force Base, Ohio.

[3] Shelton, R. D., Potter, R. A., Lacy, L., and Stuhlinger, E., "Evaluation and Analysis of Thrust Units for Power-Limited Propulsion Systems," *AIAA Journal*, Vol. 2, No. 4, April 1964, pp. 682–685.

[4] Hunter, R. E., "Theoretical Considerations of Nonuniformly Charged Expellant Beams," ARL-60-138, 1960, Aerospace Research Laboratory, Wright-Patterson Air Force Base, Ohio.

[5] Stark, K. W. and Sherman, A., "Research and Development in Needle and Slit Colloid Thrusters," X-734-68-460, 1968, NASA.

[6] Geis, J. W., "Diagnostics of a Low-Specific-Charge Colloid Ion Beam," AFAPL-TR-69-13, 1969, Aero Propulsion Labs., Wright-Patterson Air Force Base, Ohio.

[7] Geis, J. W. and Turner, J. M., "Beam Distribution Effects on Colloid Engine Performance," AIAA Paper 70-1109, Stanford, Calif., 1970.

[8] Hepburn, J. D., Chute, F. S., and Vermeulen, F. E., "Visual Display of the Spatial Distribution of Colloidal Particle Beams," *AIAA Journal*, Vol. 11, No. 3, March 1973, pp. 370–372.

[9] Dingman, E. H., "A Hypervelocity Microparticle Linear Accelerator for use in Micrometeoric Simulation," *IEEE Transactions on Nuclear Science*, Vol. NS-12, June 1965, pp. 544–549.

[10] Friichtenicht, J. F., "Micrometeoroid Simulation using Nuclear Accelerator Techniques," *Nuclear Instruments and Methods*, Vol. 28, July 1964, pp. 70–78.

[11] Harrison, E. R., "The Problem of Producing Energetic Macrons," *Plasma Physics*, Vol. 9, March–April 1967, pp. 183–191.

Measured Three-Dimensional Effects in Transonic Airfoil Testing

F. X. HURLEY*
McDonnell Douglas Corporation, St. Louis, Mo.

DURING a series of tests conducted to examine the flowfield of a supercritical airfoil, the issue of deviation from two-dimensionality was examined. Earlier surface flow visualization data[1] had provided an indication of the difficulty in attaining spanwise uniform flow.

Received August 7, 1974. This research was conducted under the McDonnell Douglas Independent Research and Development Program in cooperation with the NASA Ames Research Center.

Index category: Research Facilities and Instrumentation.

* Scientist, McDonnell Douglas Research Laboratories. Member AIAA.

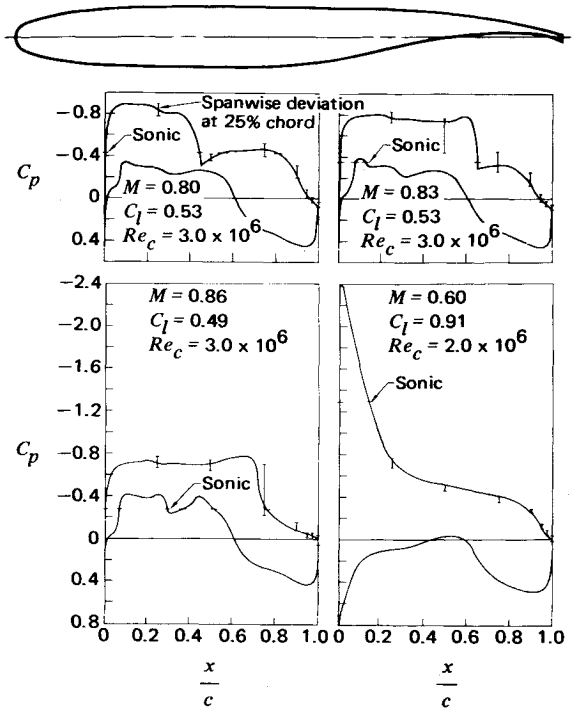

Fig. 1 Typical pressure distributions showing spanwise pressure deviation within $-1.25 \leq y/c \leq 1.25$ at various x/c stations.

The experiments were conducted in the NASA Ames Research Center Two-by-Two-Foot Transonic Wind Tunnel, which is a continuous-flow facility re-engineered specifically for airfoil section testing. The floor and ceiling have baffled slots, and insertable, solid plane sidewalls are fitted with rotating, glass disks to support the model and permit spark Schlieren photographs. A complete probe traversing capability has been added. Based on a 6 in. chord, a typical long-run Reynolds number is 3×10^6. There is no sidewall boundary-layer control; the large aspect ratio (four) is relied upon to produce a sizable region of spanwise uniform flow. In the tests reported herein, a heavily pressure-instrumented model (0.016 in. o.d. tubing) with a leading edge transition band was used.

Figure 1 presents center-span pressure distributions together with measured spanwise variances, for several Mach numbers. The deviations are worse for the essentially transonic cases than for the essentially subsonic case ($M = 0.60$). The magnitudes of some of the variances can be accounted for only by postulating a spanwise warpage of the shock wave. This is especially true of the $M = 0.83$ case. In the interval $M = 0.81$ to 0.84, the shock moves rapidly toward the trailing edge. That is to say, the shock wave position is very sensitive to flow conditions. At $M = 0.86$, it has caused substantial rearward separation and is relatively stationary.

Figure 2 shows a pair of spark Schlieren photographs (taken consecutively, a few seconds apart) at nominally identical $M = 0.82$ conditions. Since the illumination time is of the order of microseconds, these should be regarded as instantaneous images. Two phenomena may be noted: 1) the shock waves consist of diffuse patterns, and 2) the patterns are different in the two photos. From these observations, it is concluded that the shock-wave front is unsteady and is distorted in the spanwise dimension at any particular instant. The pressure tap readings of Fig. 1 represent the time-averaged component of the distortion. (This model was also instrumented with several high frequency response transducers to trace pressure fluctuations, and these data will be reported separately.)

Figure 3 presents spanwise distributions of trailing edge pressure for several flow conditions. The nonuniformity is greater

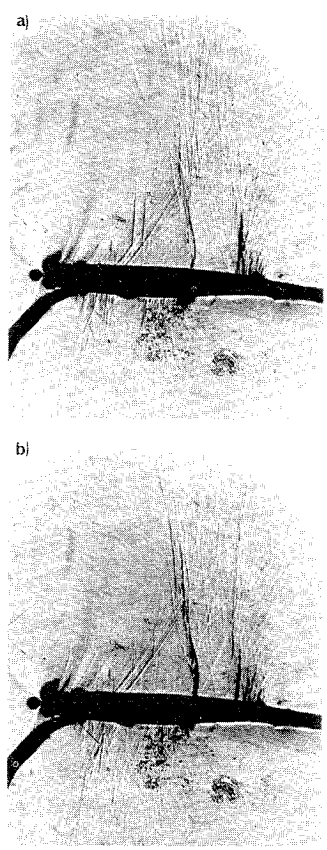

Fig. 2 Schlieren photographs comparing instantaneous shock-wave patterns at nominally identical flow conditions: $M = 0.82$, $C_l = 0.53$, $Re_c = 3.0 \times 10^6$.

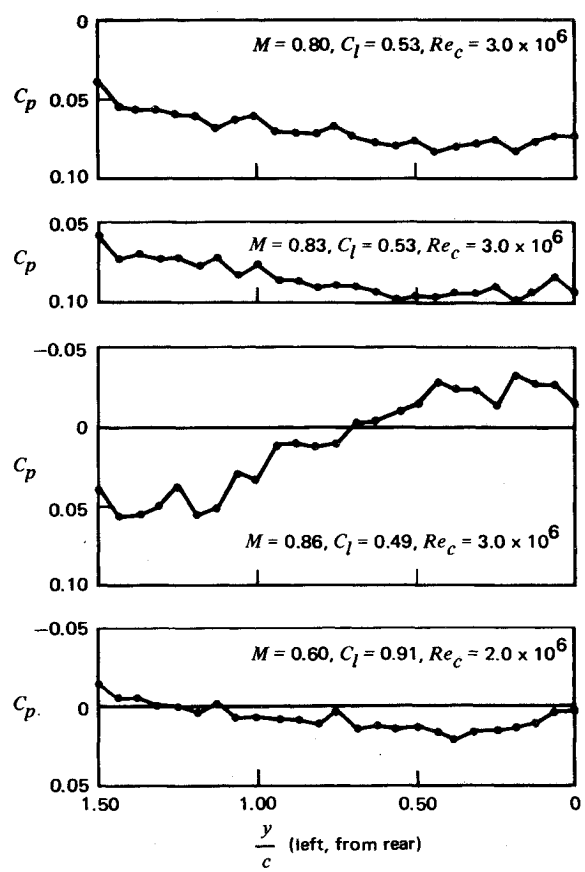

Fig. 3 Trailing-edge pressure variation in the spanwise direction. ($y/c = 0$ is center span.)

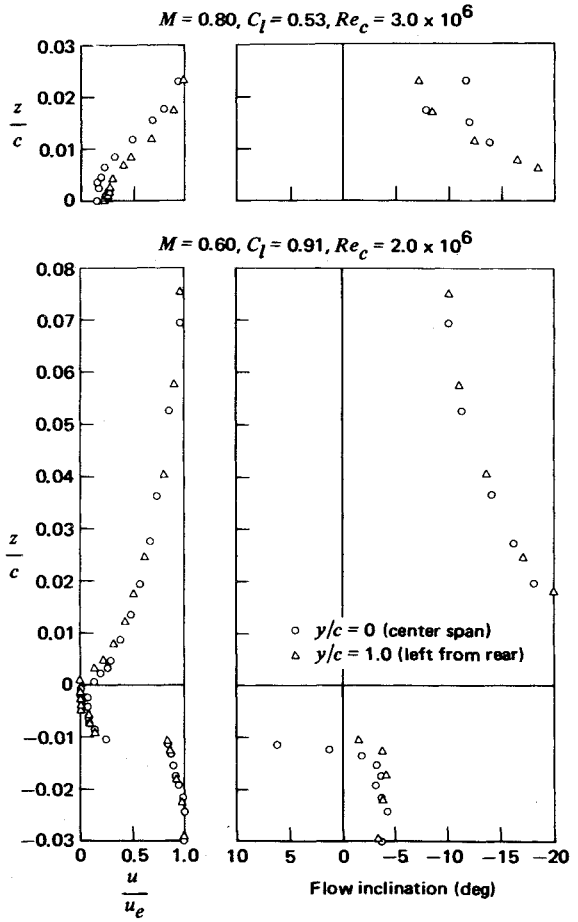

Fig. 4 Trailing-edge vector velocity profiles at different spanwise stations.

for the higher Mach numbers, especially for $M = 0.86$. The jaggedness of this plot demonstrates a cellular spanwise separation pattern, as described qualitatively by the surface flow data of Ref. 1. A clearly separated boundary-layer profile was measured on the trailing edge upper surface at the center-span location ($y/c = 0$), where the $C_{p_{te}}$ is negative.

Figure 4 compares spanwise-displaced upper surface trailing edge boundary-layer profiles for both $M = 0.60$ and $M = 0.80$. A triple-tube pressure probe with a tip depth of 0.08 mm, developed for this series to yield velocity vector data, was employed. It is seen that the spanwise deviation is much greater at the higher Mach number, whether measured by speed or by angularity. (This was the case despite the fact that the lower Mach number case carries a higher C_l, which is manifest in a larger over-all pressure rise and a much thicker upper surface boundary layer.)

The main conclusion from the data discussed herein is that significant three-dimensional effects occur in transonic airfoil tests, even for an aspect ratio of four. This is especially true at the supercritical Mach numbers, for which lateral propagation of disturbances is effective. Onset of trailing edge separation is cellular. These observations do not necessarily preclude the existence of approximately two-dimensional flow at any one spanwise section, for spanwise gradients may not be large; however, they indicate the importance of obtaining all measurements at a single spanwise location, e.g., chordwise surface pressure distributions (lift) and wake total pressure profiles (drag). In fact, C_l rather than α is the independent variable to be used, and the observed spanwise variations may be viewed as representing primarily spanwise differences in effective section angle of attack.

References

[1] Gregory, N., Quincy, V. G., O'Reilly, C. L., and Hall, D. J., "Progress Report on Observations of Three-Dimensional Flow Patterns Obtained during Stall Development on Aerofoils, and on the Problem of Measuring Two-Dimensional Characteristics," Aero. Rept. 1309, 1970, National Physical Lab., England.

Separation of Turbulent Boundary Layer on a Lifting Cylinder

N. R. KESHAVAN*
University of Southampton, Southampton, England

Nomenclature

b = width of the slot
d = diameter of the cylinder
ρ = density of the fluid
ν = kinematic viscosity of the fluid
θ = angular position from the slot
θ_{SL} = angular position of the slot measured from the freestream
C_J = jet momentum coefficient = jet momentum/freestream dynamic head

Introduction

LIFT can be generated on a circular cylinder with its axis normal to an airflow by blowing a sheet of air tangentially around the surface from a narrow slot or slots. Such a method has been attempted by Cheeseman[1,2] to generate lift on a rigid helicopter rotor and on a parkable rotor aircraft. The air injected through the slot re-energizes the boundary layer and delays its separation. The purpose of this Note is to study the flow beyond the slot until the flow separates. A similar problem of the Coanda effect on a cylinder has been studied by Newman.[3] It is observed there that the boundary-layer flow attaches itself up to large values of θ and separates. At high Reynolds numbers the point of separation becomes invariant.

Along with the parameters governing the flow beyond the slot in the Coanda effect on a cylinder one can recognize in the present problem of a lifting circular cylinder the additional parameters of jet momentum coefficient and the position of the slot governing the flow beyond the slot.

Dimensional Analysis

The parameters sufficient to define the flow after the slot on a lifting cylinder in an incompressible flow are $P - p_{SL}$ = the supply pressure related to the static pressure outside the slot, b, d, ρ, ν, θ, θ_{SL}, C_J. The surface pressure p_s at any angular position θ may be related nondimensionally to these parameters as,

$$\frac{p_{SL} - p_S}{P - p_{SL}} = f\left[\frac{\theta}{\theta_{SL}}, \frac{b}{d}, \left\{\frac{(P - p_{SL})}{\rho\nu^2} bd\right\}^{1/2}, C_J^{1/2}\right]$$

At some distance downstream of the slot one can expect the flow to become independent of the parameters $P - p_{SL}$ and b separately and depend on the product $(P - p_{SL})b$. Therefore

$$\frac{(p_{SL} - p_s)}{(P - p_{SL})} \frac{d}{b} = f\left[\frac{\theta}{\theta_{SL}}, \left\{\frac{(P - p_{SL})bd}{\rho\nu^2}\right\}^{1/2}, C_J^{1/2}\right]$$

Received August 5, 1974. This work is supported by the Science Research Council, U.K. The author wishes to thank I. C. Cheeseman for the helpful suggestions.

Index categories: Boundary-Layers and Convective Heat Transfer — Turbulent; Jets, Wakes, and Viscid-Inviscid Flow Interactions.

* Research Assistant, Department of Aeronautics and Astronautics.